Geochemical Perspectives Letters

© 2021 The Authors
Published by the European Association of Geochemistry

A genetic metasomatic link between eclogitic and peridotitic diamond inclusions

S. Mikhail[1*], M. Rinaldi[1], E.R. Mare[1], D.A. Sverjensky[2]

OPEN ACCESS

doi: 10.7185/geochemlet.2111

Abstract

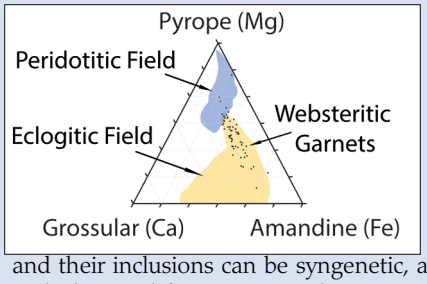

Diamond inclusions sample the otherwise inaccessible archive of Earth's deep interior. The geochemical and petrological diversity of diamond inclusions reflects either pre-metasomatic upper mantle heterogeneity or metasomatism coeval with diamond formation. We focus on the origin of lithospheric garnet and clinopyroxene inclusions by simulating metasomatic reactions between eclogitic fluids and mantle peridotites at 5 GPa, 1000 °C, and across a range of redox conditions ($\log fO_2 = -1$ to -6 ΔFMQ). Our results demonstrate that fluid-rock interaction can result in the formation of eclogitic, websteritic, and peridotitic silicates from a single fluid during a single diamond-forming metasomatic event. Ergo, the petrogenesis of diamond and their inclusions can be syngenetic, and the petrological diversity of diamond inclusions can reflect metasomatism coeval with diamond formation. Furthermore, during the metasomatism, refractory peridotite can be converted to fertile websterite which could become a pyroxenitic mantle source for oceanic basalts.

Received 24 November 2020 | Accepted 4 March 2021 | Published 24 March 2021

Introduction

Mineral inclusions in diamonds provide the geological context for diamond formation. These invaluable samples reveal that diamond formation spans more than 75 % of Earth's history (Gurney *et al.*, 2010) with most diamonds forming in the keel of the sub-continental lithospheric mantle (120–180 km; Stachel and Harris, 2008). The diversity of the petrological characteristics of diamond-hosted mineral inclusions either reflect [1] pre-metasomatic mineralogical heterogeneity in the upper mantle (Cartigny *et al.*, 2001; Nestola *et al.*, 2017), [2] fluid (Mikhail *et al.*, 2019a,b) and/or melt metasomatism (Aulbach *et al.*, 2002; Kiseeva *et al.*, 2016) coeval with diamond formation, or [3] a combination of both options. The ambiguity arises because the relationship between diamond and inclusion can be protogenetic (Nestola *et al.*, 2017) or syngenetic (Harris, 1968; Mikhail *et al.*, 2019a). We proceed here without assuming either a single protogenetic or syngenetic origin for all diamond inclusions.

Diamond-hosted mineral inclusions are diverse, including, but not limited to, sulfides, silicates, oxides, carbonates, and metallic phases (Stachel and Harris, 2008) and several of these mineral families can be sub-divided into three groups, termed inclusion paragenesis. These are [1] peridotitic (*i.e.* Cr-rich pyrope, diopside, enstatite, olivine), [2] eclogitic (*i.e.* Cr-poor pyrope-almandine, Na-rich omphacite), and [3] websteritic (intermediate compositions; Meyer and Boyd, 1972; Sobolev *et al.*, 1973; Gurney *et al.*, 1984) (Fig. 1a–d). The assignment of inclusion paragenesis is an empirical and subjective classification scheme which does not inform on process, *sensu stricto*. Herein, we focus on garnet and clinopyroxene data because these two inclusion types are present in significant abundances in all three paragenetic groups. The boundaries between peridotitic and eclogitic suites are only as clear as the contrast between the symbol shape and colour selected for the plot (Fig. 1a–d). For example, there is less of a distinction between peridotitic and eclogitic clinopyroxenes than is apparent for peridotitic and eclogitic garnets (Fig. 1a–d). In Figure 1c,d it can be seen that garnets and clinopyroxenes show an apparent continuum between the peridotitic and eclogitic suites charted by websteritic garnets (Fig. 1). Herein, we examine two key assumptions: [1] the different silicate inclusion parageneses are genetically distinct, and [2] silicate inclusion and host diamond paragenesis are syngenetic.

Methods and Results

Modelling approach. Our conceptual geologic model involves a fluid that is initially in equilibrium with a mafic eclogite migrating and encountering peridotite with which it is not in equilibrium. As a consequence, irreversible chemical mass transfer occurs. This model is analogous to a fluid migrating from a subducting slab and metasomatising the sub-continental lithospheric mantle. Alternatively, the source of the fluid could be upwelling transition zone (*i.e.* a plume), exsolving water when hydrous wadsleyite converts to olivine + H_2O and the fluid phase would rise buoyantly. We built on the long-standing tradition in theoretical aqueous geochemistry of modelling irreversible chemical mass transfer in crustal hydrothermal systems (Helgeson, 1970, 1979; Sverjensky, 1984, 1987). Here we used the aqueous speciation and solubility code EQ3 and the chemical

1. School of Earth and Environmental Sciences, University of St. Andrews, UK
2. Department of Earth and Planetary Sciences, Johns Hopkins University, USA
* Corresponding author (email: sm342@st-andrews.ac.uk)

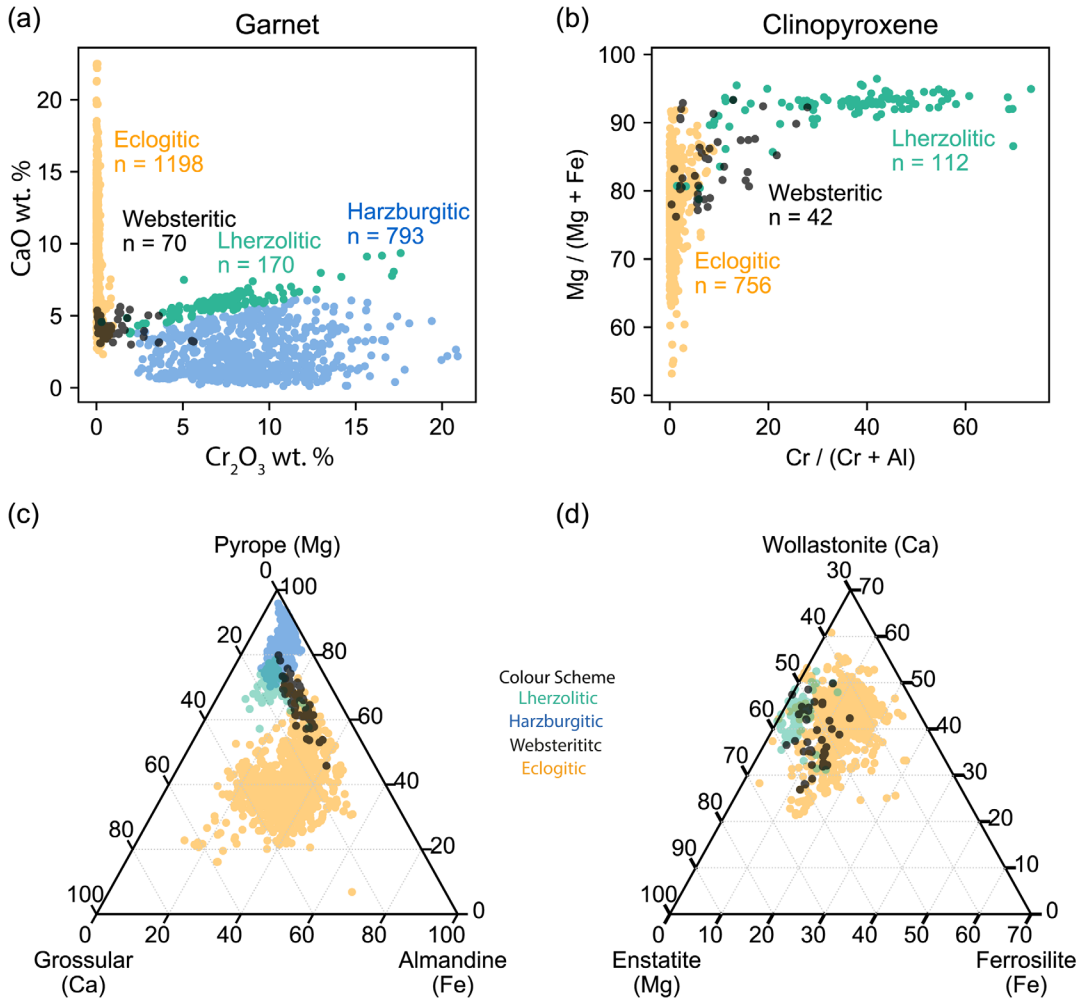

Figure 1 Inclusion parageneses (**a**,**b**) and end member compositions for garnets (**c**) and clinopyroxenes (**d**) from mantle diamond inclusions. Diamond inclusion data are from numerous sources provided in the Supplementary Information. Inclusion parageneses were assigned based on the original publisher's characterisation (see Supplementary Information). Ternaries plotted using the Python package python-ternary (Harper *et al.*, 2019).

mass transfer code EQ6 (Wolery, 1992) modified for upper mantle temperatures and pressures using thermodynamic data from the extended Deep Earth Water model calibrated with experimental solubilities (Huang and Sverjensky, 2019) previously applied to the formation of Panda diamonds (Huang and Sverjensky, 2020). More detail is given in the Supplementary Information. We ran a series of models to simulate the reactions between eclogitic fluids and a variety of lherzolite, harzburgite, and dunite compositions (Tables 1, S-5) using empirical data for peridotites from the compilation of Pearson and Wittig (2014).

Model parameterisation. The input variables are the initial fluid geochemistry, and the abundances and solid solution compositions of minerals in the initial rock, with a fixed pressure of 5 GPa and fixed temperature of 1000 °C. The initial fluids were based on a calibration of the fluid chemistry in equilibrium with a mafic eclogitic measured by Kessel *et al.* (2015) as documented in Huang and Sverjensky (2019) (Table S-1). We assumed ideal site mixing of pyrope, almandine, and grossular in garnet composition and a non-ideal mixing of diopside, hedenbergite, and clinoenstatite in clinopyroxene previously calibrated using known mineral and fluid chemistries to simulate diamond formation beneath the Panda mine in the Slave craton (NW Canada) at 950 °C and 4.5 GPa (Huang and Sverjensky, 2020). The pressure-temperature conditions adopted here (5 GPa and 1000 °C) are relevant to lithospheric diamond formation (Stachel and Harris, 2008). The temperature of 1000 °C is at the lower end of natural systems, where the average inclusion entrapment temperature is 1155 ± 105 °C ($n = 444$; Stachel and Luth, 2015). The initial oxygen fugacity (fO_2) of the model fluids was varied from −1 to −6 log units relative to the Fayalite-Magnetite-Quartz reaction (abbreviated to ΔFMQ), a greater range than is calculated from lithospheric diamond inclusions (Stachel and Luth, 2015). Representative initial fluids are given in Tables S-1 and S-2. The model outputs the evolving chemistry of the fluid and the metasomatic minerals finishing when the fluid finally equilibrates with the initial rock. The final fluid compositions and modal abundances of the minerals produced are shown by representative results in Figures 2, 3 and Tables 1, S-3–S-5 (input and output files are available at https://doi.org/10.17630/32ebd3c0-bba6-4aa1-9b6d-c53a0a3b61e0).

The Nature of Diamond Inclusion Formation

Connecting eclogitic to peridotitic inclusions along a single reaction pathway. Fluid-rock interaction results in the compositional evolution of the fluid phase coupled to the continual precipitation of mineral phases with progressively more Mg-rich

Table 1 Key parameters for representative metasomatic mass transfer modes presented in Figures 2, 3. The pressure and temperature for all runs was fixed at 5 GPa and 1000 °C with the starting fluid fO_2 and fluid pH fixed at ΔFMQ −3 and pH 5.0, respectively. ΔfO_2 and ΔpH express changes in the final fluid relative to the initial. Note that these changes are very small even though the mineralogical changes in the rock are very large. A larger suite of results is provided in Table S-5.

Run	pH	ΔfO_2	ΔpH	Initial Rock	Initial Mineralogy (vol %)	Final Mineralogy (vol %)	Final Rock
Run 27	5	0.35	0.13	Lherzolite	Olivine (54.80), Opx (20.02), Cpx (20.20), Garnet (4.98)	Olivine (0.11), Opx (58.62), Cpx (31.71), Garnet (7.42), Diamond (0.05), Magnetite (2.09)	Websterite
Run 45	5	−0.42	0.14	Lherzolite + aragonite	Olivine (52.52), Opx (19.18), Cpx (19.36), Garnet (4.77), Aragonite (4.17)	Olivine (0.09), Opx (40.55), Cpx (49.48), Garnet (7.62), Diamond (0.07), Magnetite (2.19)	Websterite
Run 75	5	−0.06	0.14	Dunite + aragonite	Olivine (81.80), Opx (4.43), Cpx (4.62), Garnet (4.42), Aragonite (4.73)	Olivine (0.22), Opx (20.69), Cpx (62.87), Garnet (13.28), Diamond (0.06), Magnetite (2.88)	Websterite
Run 93	5	−0.06	0.14	Harzburgite + aragonite	Olivine (67.89), Opx (22.73), Garnet (4.78), Aragonite (4.60)	Olivine (0.15), Opx (46.34), Cpx (39.92), Garnet (10.92), Diamond (0.07), Magnetite (2.60)	Websterite
Run 111	5	−0.12	0.13	Dunite	Olivine (85.86), Opx (4.65), Cpx (4.85), Garnet (4.64)	Opx (58.29), Cpx (26.61), Garnet (12.40), Diamond (0.03), Magnetite (2.67)	Websterite
Run 117	5	−0.12	0.12	Harzburgite	Olivine (71.16), Opx (23.83), Garnet (5.01)	Olivine (0.13), Opx (73.46), Cpx (13.53), Garnet (10.40), Diamond (0.04), Magnetite (2.44)	Websterite

garnet and clinopyroxene compositions (Fig. 2a–d). In fact, the major element geochemistry of garnets precipitated in our models traverses from eclogitic to peridotitic along the websteritic 'bridge' during a single reaction pathway (Fig. 3a). Importantly, it can be seen in Figure 3a that reaction pathways in lherzolite, harzburgite, and dunite follow the same compositional trend. Metasomatism of a single peridotite by a single eclogitic fluid will result in the progressive precipitation of garnets starting with eclogitic, then websteritic, and finally pyrope-rich peridotitic compositions (Fig. 3a). A similar observation is true for clinopyroxenes, where our models all travel from deep inside the eclogitic field and cross over the (poorly defined) websteritic data cluster and into the (also poorly defined) peridotitic cluster along a single reaction pathway (Fig. 3b). Our results for garnet and clinopyroxene compositional trends may not apply to all diamond-hosted mineral inclusions, but they demonstrate that the paragenesis for the inclusion and host diamond can be syngenetic, and that the different inclusion parageneses can be genetically related and preserve a reaction pathway. Therefore, and on occasion, inclusion paragenesis does not serve as a *bona fide* proxy for provenance. For example, a peridotitic inclusion can precipitate from an eclogitic fluid, while an eclogitic inclusion will precipitate from an eclogitic fluid within a peridotite. Without diamond to preserve the reaction products as inclusions there would be no evidence for this pathway (*i.e.* the websteritic bridge) because the high temperatures of the mantle are in excess of the blocking temperature for these phases (Pearson and Wittig, 2014) which would result in post-formation homogenisation *via* diffusion. However, the highly refractory, low diffusivity, and inert nature of diamond, results in archives of this reaction pathway occasionally, and globally, in the geochemistry of diamond inclusions (Fig. 3a,b).

The formation of diamond along single reaction pathways (shown in Fig. 2b) involving subducted fluids reacting with ambient mantle peridotite, as presented here, is consistent with the several observations for the geochemistry of diamonds and their inclusions. Our models provide a single mechanistic explanation for the situation where single natural diamonds host disequilibrium inclusion assemblages, such as diamonds hosting inclusions of mixed parageneses (Gurney and Boyd, 1982; Wang, 1998; Dobosi and Kurat, 2010; Mikhail *et al.*, 2019a). Furthermore, our models satisfy some stable isotope data, such as strong isotopic evidence for the role of both mantle and crustal sources within single samples and single sample populations. For example, mantle-like high $^{3}He/^{4}He$ is observed for diamonds with crustal-like ^{15}N-enrichment and ^{13}C-depletion (Gautheron *et al.*, 2005; Mikhail *et al.*, 2019b; Timmerman *et al.*, 2019) and the occasional observation for coupled and progressive ^{13}C-depletion and ^{18}O-enrichment trends between diamond and inclusion (Schulze *et al.*, 2013).

Other Implications

Isothermal and redox neutral diamond formation. Diamond formation by the reduction or oxidation of carbon is difficult to express because lithospheric peridotites can only buffer fO_2 for systems where the fluid component is present in trace quantities (<50 ppm; Luth and Stachel, 2014). This led Stachel and Luth (2015) to propose a redox neutral mechanism where diamond forms during the cooling of a COH fluid as it crosses thermal gradient. Our data also show that diamond formation is feasible without the need for any shift in redox or pH of the fluid ($\log fO_2$ in our models shifts by ≤0.4 log units; Table 1). Contrary to the model in Stachel and Luth (2015), our dataset also demonstrates that a thermal gradient is not required. Our models predict isothermal and isobaric diamond formation during irreversible chemical mass transfer. The fundamental driving force for the metasomatism during the chemical mass transfer is provided by the initial chemical disequilibrium when a fluid leaves a mafic eclogitic rock and encounters a peridotite with which it must react.

A metasomatic origin for mantle pyroxenites. These data inadvertently predict that fluid metasomatism is a potential

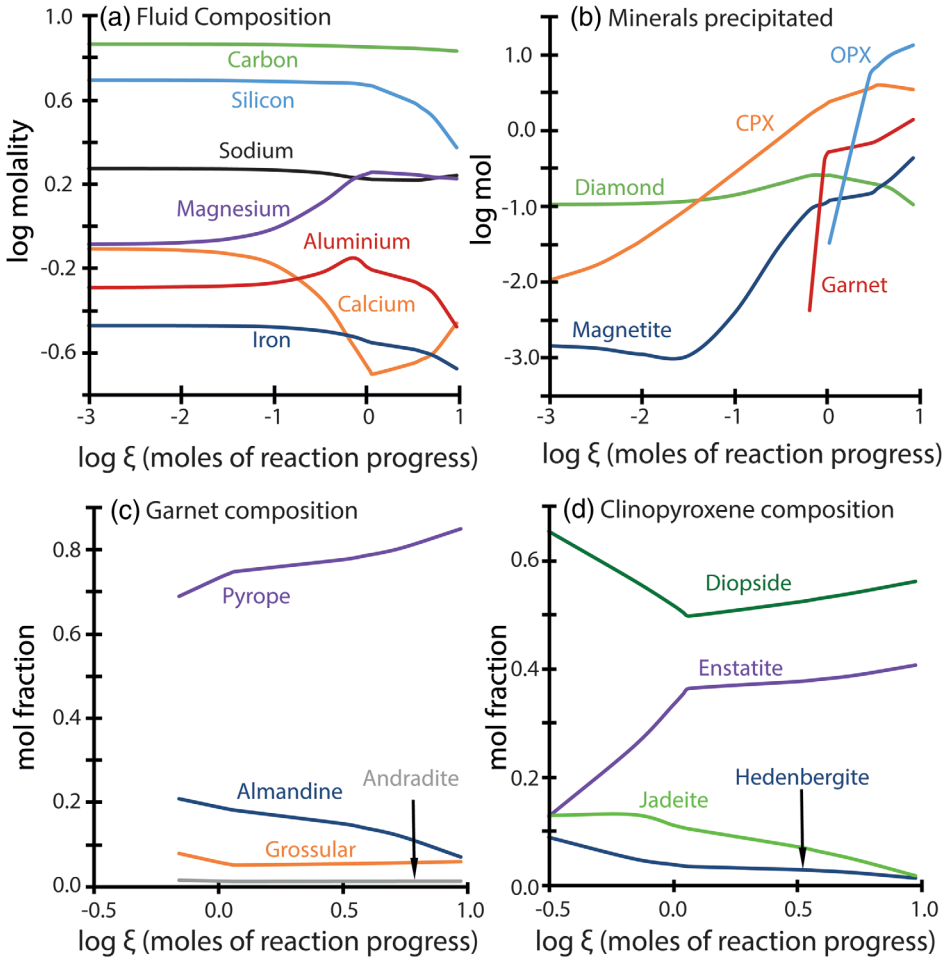

Figure 2 Model results for the reaction pathway during metasomatism of lherzolite by an eclogitic fluid (Run 27; Tables 1, S-1–S-4). Each unit of the reaction progress variable (ξ) corresponds to destruction of 1.0 mole of each of the reactant minerals *per* 1.0 kg of H_2O in the initial fluid. **(a)** Changes in the total dissolved concentration of the major elements in the fluid; **(b)** Moles of new minerals precipitated from the fluid during the continuous reaction pathway; **(c)** and **(d)** The compositions of garnets and clinopyroxenes, respectively, as a function of reaction progress. Full results for all models are provided in the output files (available upon request). Olivine precipitates in the final stage of the model (Table 1) and is therefore absent in Figure 2b. Note change in scale for the x axis for a–b *vs.* c–d.

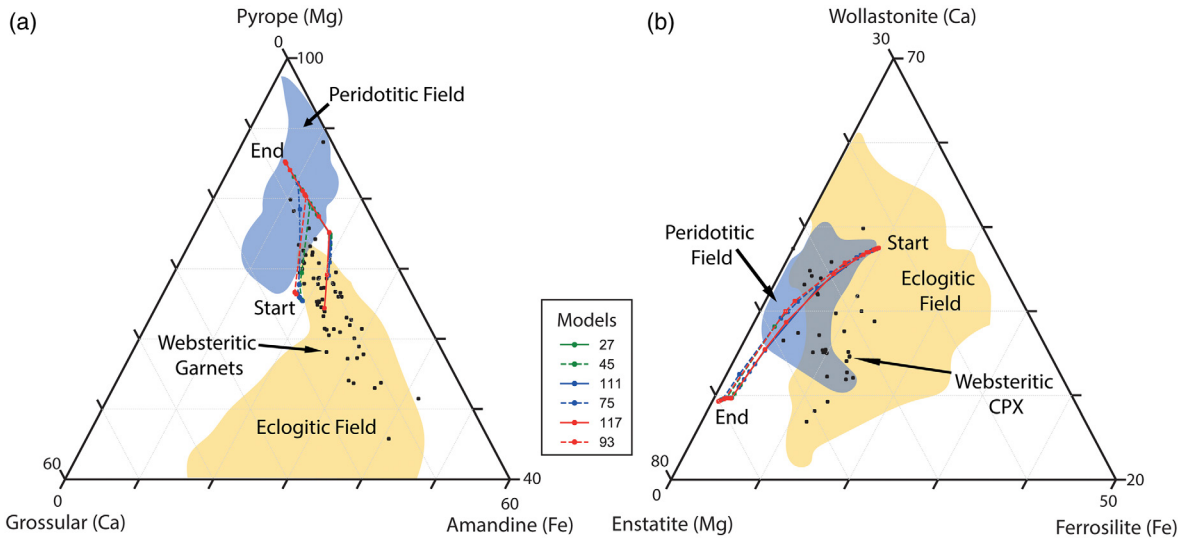

Figure 3 Selected model results for predicted **(a)** garnet and **(b)** clinopyroxene compositions during progressive metasomatism. Each model run refers to a single peridotite metasomatised by a single eclogitic fluid. Key parameters for the models shown are detailed in Tables 1, S-1–S-5, and the input and output files are available upon request.

candidate for the sub-solidus conversion of refractory peridotite into fertile websterite (Fig. 2 and Table 1). The final amount of olivine is less than 1 % in volume and produced only in the very last step of the models (Tables 1, S-5). Our models show the reaction pathway for mafic eclogitic fluids with garnet-bearing and garnet-free dunites, harzburgites, or lherzolites always results in the precipitation of a two-pyroxene dominated mineral assemblage (*i.e.* websterite; Tables 1, S-5). Interestingly, our metasomatic model producing pyroxenite and diamond is closely analogous to a pyroxenite-diamond connection previously suggested (Kiseeva *et al.*, 2016) albeit with a sub-solidus fluid rather than a melt. Furthermore, the major element geochemistry of mid-ocean ridge and ocean island basalts has been used to posit a pyroxenite-bearing mantle source (very high pyroxene to olivine ratio; Hirschmann and Stolper, 1996; Sobolev *et al.*, 2007). Thus pyroxenites produced by fluid metasomatism (this study) may not be common or vast in scale, but our model demonstrates a mechanism for the generation of a a pyroxenitic source *via* the metasomatic conversion of peridotite into websterite, without the need to champion a mechanism involving high temperature melting of refractory eclogite.

Acknowledgements

We are extremely grateful to Thomas Stachel (Univ. of Alberta) for generously sharing the extensive database for mineral inclusions in diamonds without which this study would have taken several years to complete. Funding for SM, ERM, and MR is provided by NERC standard grant (NE/PO12167/1) and UK Space Agency Aurora grant (ST/T001763/1). Funding for DAS is provided by the US DOE (DE-FG-02-96ER-14616) and the US NSF (EAR 1624325 and ACI 1550346). We are grateful to the constructive peer review process handled by Dr Helen Williams and provided by Dr Sonja Aulbach, Dr Janne Koorneef, and two anonymous reviewers, which improved the clarity of this contribution.

Editor: Helen Williams

Additional Information

Supplementary Information accompanies this letter at https://www.geochemicalperspectivesletters.org/article2111.

© 2021 The Authors. This work is distributed under the Creative Commons Attribution Non-Commercial No-Derivatives 4.0 License, which permits unrestricted distribution provided the original author and source are credited. The material may not be adapted (remixed, transformed or built upon) or used for commercial purposes without written permission from the author. Additional information is available at https://www.geochemicalperspectivesletters.org/copyright-and-permissions.

Cite this letter as: Mikhail, S., Rinaldi, M., Mare, E.R., Sverjensky, D.A. (2021) A genetic metasomatic link between eclogitic and peridotitic diamond inclusions. *Geochem. Persp. Let.* 17, 33–38.

References

Aulbach, S., Stachel, T., Viljoen, K.S., Brey, G.P., Harris, J.W. (2002) Eclogitic and websteritic diamond sources beneath the Limpopo Belt – is slab-melting the link? *Contributions to Mineralogy and Petrology* 143, 56–70.

Cartigny, P., Harris, J.W., Javoy, M. (2001) Diamond genesis, mantle fractionations and mantle nitrogen content: a study of $\delta^{13}C$–N concentrations in diamonds. *Earth and Planetary Science Letters* 185, 85–98.

Dobosi, G., Kurat, G. (2010) On the origin of silicate-bearing diamondites. *Mineralogy and Petrology* 99, 29–42.

Gautheron, C., Cartigny, P., Moreira, M., Harris, J.W., Allègre, C.J. (2005) Evidence for a mantle component shown by rare gases, C and N isotopes in polycrystalline diamonds from Orapa (Botswana). *Earth and Planetary Science Letters* 240, 559–572.

Gurney, J.J., Boyd, F.R. (1982) Mineral intergrowths with polycrystalline diamonds from Orapa Mine, Botswana. *Carnegie Institution of Washington Yearbook* 81, 267–273.

Gurney, J.J., Harris, J.W., Rickard, R.S. (1984) Silicate and oxide inclusions in diamonds from the Orapa mine, Botswana. In: Kornprobst, J. (Ed.) *Kimberlites II: The Mantle and Crust-Mantle Relationships*. Developments in Petrology, Elsevier, Amsterdam, 3–9.

Gurney, J.J., Helmstaedt, H.H., Richardson., S.H., Shirey, S.B. (2010) Diamonds through time. *Economic Geology* 105, 689–712.

Harper, M., Weinstein, B., tgwoodcock, Simon, C., chebee7i, Morgan, W., Knight, V., Swanson-Hysell, N., Evans, M., jl-bernal, ZGainsforth, The Gitter Badger, SaxonAnglo, Greco, M., Zuidhof, G. (2019) marcharper/python-ternary: Version 1.0.6. *Zenodo*, doi: 10.5281/zenodo.2628066.

Harris, J.W. (1968) The recognition of diamond inclusions. Part 1: syngenetic mineral inclusions. *Industrial Diamond Review* 28, 402–410.

Helgeson, H.C. (1970) A chemical and thermodynamic model of ore deposition in hydrothermal systems. In: Morgan, B.A. (Ed.) *Fiftieth Anniversary Symposia: Mineralogy and Petrology of the Upper Mantle; Sulfides; Mineralogy and Geochemistry of Non-Marine Evaporites*. Special Paper No. 3, Mineralogical Society of America, Washington, D.C., 155–186.

Helgeson, H.C. (1979) Mass transfer among minerals and hydrothermal solutions. In: Barnes, H.L. (Ed.) *Geochemistry of Hydrothermal Ore Deposits*. Wiley, New York, 568–610.

Hirschmann, M.M., Stolper, E.M. (1996) A possible role for garnet pyroxenite in the origin of the 'garnet signature' in MORB. *Contributions to Mineralogy and Petrology* 124, 185–208.

Huang, F., Sverjensky, D.A. (2019) Extended Deep Earth Water Model for predicting major element mantle metasomatism. *Geochimica et Cosmochimica Acta* 254, 192–230.

Huang, F., Sverjensky, D.A. (2020) Mixing of carbonatitic into saline fluid during Panda diamond formation. *Geochimica et Cosmochimica Acta*, 284, 1–20.

Kessel, R., Pettke, T., Fumagalli, P. (2015) Melting of metasomatized peridotite at 4–6 GPa and up to 1200 °C: an experimental approach. *Contributions to Mineralogy and Petrology* 169, 37.

Kiseeva, E.S., Wood, B.J., Ghosh, S., Stachel, T. (2016) The pyroxenite-diamond connection. *Geochemical Perspectives Letters* 2, 1–9.

Luth, R.W., Stachel, T. (2014) The buffering capacity of lithospheric mantle: implications for diamond formation. *Contributions to Mineralogy and Petrology* 168, 1083.

Meyer, H.O.A., Boyd, F.R. (1972) Composition and origin of crystalline inclusions in natural diamonds. *Geochimica et Cosmochimica Acta* 36, 1255–1273.

Mikhail, S., Crosby, J.C., Stuart, F.M., DiNicola, L., Abernethy, F.A.J. (2019b) A secretive mechanical exchange between mantle and crustal volatiles revealed by helium isotopes in ^{13}C-depleted diamonds. *Geochemical Perspectives Letters* 11, 39–43.

Mikhail, S., McCubbin, F.M., Jenner, F.E., Shirey, S.B., Rumble, D., Bowden, R. (2019a) Diamondites: evidence for a distinct tectono-thermal diamond-forming event beneath the Kaapvaal craton. *Contributions to Mineralogy and Petrology* 174, 71.

Nestola, F., Jung, H., Taylor, L.A. (2017) Mineral inclusions in diamonds may be synchronous but not syngenetic. *Nature Communications* 14168, doi: 10.1038/ncomms14168.

Pearson, D.G., Wittig, N. (2014) The formation and evolution of cratonic mantle lithosphere—evidence from mantle xenoliths. In: Holland, H.D., Turekian, K.K. (Eds.) *Treatise on Geochemistry*. Second edition, Elsevier, Oxford, 255–292.

Schulze, D.J., Harte, B., Page, F.Z., Valley, J.W., Channer, D.M.D., Jaques, A.L. (2013) Anticorrelation between low $\delta^{13}C$ of eclogitic diamonds and high $\delta^{18}O$ of their coesite and garnet inclusions requires a subduction origin. *Geology* 41, 455–458.

Sobolev, N.V., Lavrent'ev, Y.G., Pokhilenko, N.P., Usova, L.V. (1973) Chrome-rich garnets from the kimberlites of yakutia and their parageneses. *Contributions to Mineralogy and Petrology* 40, 39–52.

Sobolev, A.V., Hofmann, A.W., Kuzmin, D.V., Yaxley, G.M., Arndt, N.T., Chung, S.L., Danyushevsky, L.V., Elliott, T., Frey, F.A., Garcia, M.O., Gurenko, A.A., Kamenetsky, V.S., Kerr, A.C., Krivolutskaya, N.A., Matvienkov, V.V., Nikogosian, I.K., Rocholl, A., Sigurdsson, I.A., Sushchevskaya, N.M., Teklay, M. (2007) The amount of recycled crust in sources of mantle-derived melts. *Science* 316, 412–417.

Stachel, T., Harris, J.W. (2008) The origin of cratonic diamonds – constraints from mineral inclusions. *Ore Geology Review* 34, 5–32.

Stachel, T., Luth, R.W. (2015) Diamond formation – Where, when and how? *Lithos* 223, 200–220.

Sverjensky, D.A. (1984) Oil-field brines as ore-forming solutions. *Economic Geology* 79, 23–37.

Sverjensky, D.A. (1987) The role of migrating oil-field brines in the formation of sediment-hosted Cu-rich deposits. *Economic Geology* 82, 1130–1141.

Timmerman, S., Honda, M., Burnham, A.D., Amelin, Y., Woodland, S., Pearson, D.G., Jaques, A.L., Le Losq, C., Bennett, V.C., Bulanova, G.P., Smith, C.B., Harris, J.W., Tohver, E. (2019) Primordial and recycled helium isotope signatures in the mantle transition zone. *Science* 365, 692–694.

Wang, W. (1998) Formation of diamond with mineral inclusions of "mixed" eclogite and peridotite paragenesis. *Earth and Planetary Science Letters* 160, 831–834.

Wolery, T.J. (1992) *EQ3/6: A software package for geochemical modeling of aqueous systems: package overview and installation guide (version 7.0)*. Lawrence Livermore National Laboratory, University of California, Livermore, CA.

Geochemical Perspectives Letters

© 2021 The Authors
Published by the European Association of Geochemistry

A genetic link between eclogitic and peridotitic diamond inclusions

S. Mikhail, M. Rinaldi, E.R. Mare, D.A. Sverjensky

Supplementary Information

The Supplementary Information includes:

- S1. Diamond Inclusion Database
- S2. Reaction Path Modelling and the Extended Deep Earth Water Model
- Tables S-1 to S-5
- Supplementary Information References

S1. Diamond Inclusion Database

The diamond inclusion database contains meta- and geochemical data for 9118 diamond inclusions including the major element data for olivine (n = 1334), orthopyroxene (n = 446), clinopyroxene (n = 926), and garnet (n = 2628) inclusions from lithospheric mantle diamonds sourced, primarily, from Stachel and Harris (2008 and references therein) supplemented with additional and more recent datasets (Gurney and Boyd, 1982; Gurney *et al.*, 1984; Viljoen *et al.*, 1999; Jacob *et al.*, 2000; Tappert *et al.*, 2005; De Stefano *et al.*, 2009; Sobolev *et al.*, 2009; Tappert *et al.*, 2009; Bulanova *et al.*, 2010; Dobosi and Kurat, 2010; Miller *et al.*, 2014; Mikhail *et al.*, 2019).

S2. Extended Deep Earth Water Model

The Extended Deep Earth Water Model (DEW) to calculate the apparent standard partial molal Gibbs free energies of aqueous species at high pressures and temperatures using the revised Helgeson-Kirkham-Flowers (HKF) equations of state for aqueous species (Shock and Helgeson, 1988; Shock *et al.*, 1997; Sverjensky *et al.*, 1997) calibrated with experimental solubilities of eclogite and peridotite (Huang and Sverjensky, 2019; Sverjensky, 2019). Equilibrium constants for aqueous complexes calculated using the DEW model were used in the aqueous speciation, solubility, and chemical mass transfer codes EQ3 and EQ6 (modified after Wolery,

1983, 1984, 1992 for elevated temperatures and pressures) as documented in Huang and Sverjensky (2019). Our aqueous speciation model also included a model for the variable activity of water and the activity coefficients of aqueous, neutral dissolved gases such as H_2CO_3, CO_2, CH_4, CO, and C_2H_6 as functions of the solute content of the fluid (Huang and Sverjensky, 2019).

As a first step in the modeling, EQ3 was used to generate the composition and speciation of initial C-rich fluids in equilibrium with the specified mineral compositions in a mafic eclogite (Tables S-1 and S-2). We used the mafic eclogitic mineral compositions at 1000 °C and 5.0 GPa reported in Kessel *et al*. (2015). The fluid in equilibrium with these minerals measured by Kessel *et al*. was analysed theoretically in Huang and Sverjensky (2019) as part of a calibration of the thermodynamic properties of complexes of the major elements. We used this calibration, but we also adopted a variety of values for the fO_2 to ensure a range of different initial fluid chemistries.

The metasomatic interactions between these initial fluids and a variety of peridotitic substrates were simulated using the irreversible chemical mass transfer code EQ6 (results tabulated in Tables S-3–S-5). Both the initial and final rock modes are given in Table S-5. The simulations predicted the stepwise interaction of fluid and rock to yield the progressive evolution of the fluid chemistry and aqueous speciation as well as the evolution of metasomatic mineral solid solutions during reaction progress. Although the temperature and pressure of the simulations were set at 1000 °C and 5.0 GPa, preliminary calculations indicate very similar results at temperatures 100–200 °C lower and pressures 1.0–2.0 GPa lower. It should be emphasized that the initial fluid in each case is out of equilibrium with the initial peridotite reactant. During the irreversible chemical reactions, the fluid chemistry and the mineralogy, which are coupled, can therefore evolve chemically. Important parameters such as the oxygen fugacity and pH are determined throughout each run by the bulk chemistry of the reacting fluid-rock system, as is the potential for new minerals to react and even re-dissolve. All the initial reactant minerals in Table S5 are assumed to have the same relative reaction rates, which may be a reasonable assumption at the elevated temperature and pressure considered here.

The initial lherzolitic reactant minerals are progressively destroyed during reaction progress as the fluid tries to equilibrate with the rock. Each unit of the reaction progress variable (ξ) corresponds to destruction of 1.0 mole of each of the reactant minerals. The new minerals formed during the metasomatic reactions are plotted in Figs. 2a–d (main text) as functions of the logarithm of the reaction progress variable ($\log\xi$).

Supplementary Tables

Table S-1 The initial fluid composition and controls on the compositional variables.

	Eclogitic fluid (Fluid number 3)		**Eclogitic fluid** (Fluid number 4.1)		**Eclogitic fluid** (Fluid number 5)	
Variable	Concentration[a]	Set with	Concentration[a]	Set with	Concentration[a]	Set with
Na	2.50	Charge balance	1.40	Charge balance	1.40	Charge balance
Ca	1.84	Diopside (0.35)	0.66	Diopside (0.35)	0.52	Diopside (0.35)
Mg	1.65	Pyrope (0.352)	0.07	Pyrope (0.352)	0.02	Pyrope (0.352)
Fe	0.90	Almandine (0.323)	0.13	Almandine (0.323)	0.05	Almandine (0.323)
Al	1.02	Grossular (0.326)	0.79	Grossular (0.326)	0.73	Grossular (0.326)
Si	8.18	Coesite (1.0)	7.09	Coesite (1.0)	6.51	Coesite (1.0)
C	20.0	Given	20.0	Given	20.0	Given
pH	4.95	Jadeite (0.539)	4.82	Jadeite (0.539)	4.82	Jadeite (0.539)
aH_2O	0.69		0.73		0.71	
$\log fO_2$	-10.4		-11.4		-12.4	
ΔFMQ	-3.0		-4.0		-5.0	

[a] Element concentrations refer to molality (moles/kg H_2O).

Table S-2 Model aqueous speciation results for the ten most abundant aqueous species (molal) in the initial fluid and the pH and fO_2.

Eclogitic fluid (Fluid number 3)		**Eclogitic fluid** (Fluid number 4.1)		**Eclogitic fluid** (Fluid number 5)	
Variable	Concentration[b]	Variable	Concentration[b]	Variable	Concentration[b]
H_2CO_3 (aq)	6.45	CH_4 (aq)	8.49	CH_4 (aq)	13.08
$HCOO^-$	2.74	Ethane (aq)	2.83	Ethane (aq)	2.38
CH_4 (aq)	2.10	H_4SiO_4 (aq)	1.46	H_4SiO_4 (aq)	1.38
$Mg(SiO_2)(HCO_3)^+$	1.63	Na^+	1.23	Na^+	1.26
$Ca(HCOO)^+$	1.39	Propane (aq)	1.15	$H_8Si_3O_{10}$ (aq)	0.93
H_4SiO_4 (aq)	1.30	$H_8Si_3O_{10}$ (aq)	1.03	$Al(OH)_3OSi(OH)_3^-$	0.71
$NaHCO_3$	1.26	Ethanol (aq)	0.87	$H_3SiO_4^-$	0.56
Na^+	1.10	$Al(OH)_3OSi(OH)_3^-$	0.76	OH^-	0.55
$Al(OH)Si(OH)^-$	0.99	$H_3SiO_4^-$	0.58	Propane (aq)	0.53
$Fe(HCOO)^+$	0.87	OH^-	0.55	$Ca(H_3SiO_4)^+$	0.51
pH	4.95	pH	4.82	pH	4.82
logfO_2	-10.4	**logfO_2**	-11.5	**logfO_2**	-12.4
ΔFMQ	-3.0	**ΔFMQ**	-4.1	**ΔFMQ**	-5.0

[b] Aqueous species concentrations refer to molality (moles/kg H_2O).

Table S-3 The final fluid compositions for Run 27, 28 and 29 (see Table S-5).

	Final fluid (initial ΔFMQ -3.0)		**Final fluid (initial ΔFMQ -4.1)**		**Final fluid (initial ΔFMQ -5.0)**	
	Model 27 Lherzolite + Fluid number 3		Model 28 Lherzolite + Fluid Number 4.1		Model 29 Lherzolite + Fluid Number 5	
Variable	Concentration[a]	wt% oxide	Concentration[a]	wt% oxide	Concentration[a]	wt% oxide
Na	1.75	3.36	1.13	1.93	1.18	1.87
Ca	0.35	1.21	0.13	0.40	0.09	0.26
Mg	1.68	4.19	0.31	0.69	0.27	0.56
Fe	0.21	0.93	0.09	0.36	0.03	0.11
Al	0.33	1.04	0.20	0.56	0.19	0.49
Si	2.37	8.81	0.84	2.77	0.78	2.39
C	6.83	18.6	15.84	38.3	19.3	43.3
H		61.9		55.0		51.0
pH	5.09		4.98		4.99	
aH_2O	0.86		0.79		0.76	
logfO_2	-10.0		-11.7		-12.3	
Δ**FM**Q	-2.6		-4.3		-4.9	

[a] Element concentrations refer to molality (moles/kg H_2O).

Table S-4 Model aqueous speciation results for the ten most abundant aqueous species (molal) in the final fluid for Run 27, 28 and 29 (see Table S-5).

Final fluid (initial ΔFMQ -3.0)		**Final fluid (initial ΔFMQ -4.1)**		**Final fluid (initial ΔFMQ -5.0)**	
Model 27 Lherzolite + Fluid number 3		Model 28 Lherzolite + Fluid Number 4.1		Model 29 Lherzolite + Fluid Number 5	
Variable	Concentration[b]	Variable	Concentration[b]	Variable	Concentration[b]
H_2CO_3 (aq)	2.80	CH_4 (aq)	8.26	CH_4 (aq)	11.42
$Mg(SiO_2)(HCO_3)^+$	1.35	Ethane (aq)	2.12	Ethane (aq)	2.02
OH^-	1.05	Na^+	0.94	Na^+	0.99
$HCOO^-$	1.02	OH^-	0.74	OH^-	0.76
$NaHCO_3$ (aq)	0.82	Propane (aq)	0.66	Propane (aq)	0.43
Na^+	0.74	Ethanol (aq)	0.52	H_4SiO_4 (aq)	0.30
H_4SiO_4 (aq)	0.35	H_4SiO_4 (aq)	0.33	$Mg(OH)_2$ (aq)	0.27
$Mg(OH)_2$ (aq)	0.33	$Mg(OH)_2$ (aq)	0.28	Ethanol (aq)	0.25
$Al(OH)Si(OH)^-$	0.30	NaOH (aq)	0.18	NaOH (aq)	0.19
$Ca(HCOO)^+$	0.28	$Al(OH)Si(OH)^-$	0.17	$Al(OH)Si(OH)^-$	0.16
pH	5.09	pH	4.98	pH	4.99
log*f*O$_2$	-10.0	**log*f*O$_2$**	-11.7	**log*f*O$_2$**	-12.3
ΔFMQ	-2.6	**ΔFMQ**	-4.3	**ΔFMQ**	-4.9

[b] Aqueous species concentrations refer to molality (moles/kg H_2O).

Table S-5 Key parameters for representative metasomatic mass transfer modes undertaken during this study. The pressure and temperature for all runs was fixed at 5 GPa and 1000 °C with the starting fluid fO_2 and fluid pH fixed at ΔFMQ -3 and 5.0, respectively. ΔfO_2 and ΔpH express changes in the final fluid relative to the initial. Note that these changes are very small even though the mineralogical changes in the rock are very large. Runs in bold are reproductions of data from Table 1 for the sake of completeness.

Run	P GPa	T °C	logfO_2 ΔFMQ	pH	ΔlogfO_2	ΔpH	Initial Rock	Initial Mineralogy (vol %)	Final mineralogy (vol %)
3	5	1000	-3	5	0.36	0.14	Lherzolite (no garnet)	Olivine (59.99), Opx (19.80), Cpx (20.21)	Olivine (0.10), Opx (63.32), Cpx (32.77), Garnet (1.65), Diamond (0.05), Magnetite (2.11)
9	5	1000	-3	5	0.42	0.15	Lherzolite + aragonite (no garnet)	Olivine (57.43), Opx (18.95), Cpx (19.34), Aragonite (4.28)	Olivine (0.10), Opx (43.79), Cpx (52.30), Garnet (1.54), Diamond (0.07), Magnetite (2.20)
27	**5**	**1000**	**-3**	**5**	**0.35**	**0.14**	**Lherzolite**	**Olivine (54.80), Opx (20.02), Cpx (20.20), Garnet (4.98)**	**Olivine (0.11), Opx (58.62), Cpx (31.71), Garnet (7.42), Diamond (0.05), Magnetite (2.09)**
28	5	1000	-4.1	5	-0.30	0.16	Lherzolite	Olivine (54.80), Opx (20.02), Cpx (20.20), Garnet (4.98)	Olivine (0.05), Opx (67.44), Cpx (24.22), Garnet (8.29)
29	5	1000	-5	5	0.18	0.09	Lherzolite	Olivine (54.80), Opx (20.02), Cpx (20.20), Garnet (4.98)	Olivine (0.06), Opx (66.28), Cpx (24.89), Garnet (8.77)
33	5	1000	-3	5	0.35	0.14	Lherzolite (10 vol.% garnet)	Olivine (50.19), Opx (20.09), Cpx (19.92), Garnet (9.80)	Opx (54.72), Cpx (30.63), Garnet (12.49), Diamond (0.06), Magnetite (2.10)
39	5	1000	-3	5	0.35	0.14	Lherzolite (15 vol.% garnet)	Olivine (45.08), Opx (19.89), Cpx (19.87), Garnet (15.16)	Olivine (0.10), Opx (50.35), Cpx (29.86), Garnet (17.54), Diamond (0.06), Magnetite (2.09)
45	**5**	**1000**	**-3**	**5**	**-0.42**	**0.14**	**Lherzolite + aragonite**	**Olivine (52.52), Opx (19.18), Cpx (19.36), Garnet (4.77), Aragonite (4.17)**	**Olivine (0.09), Opx (40.55), Cpx (49.48), Garnet (7.62), Diamond (0.07), Magnetite (2.19)**
46	5	1000	-4.1	5	-0.20	0.15	Lherzolite + aragonite	Olivine (52.52), Opx (19.18), Cpx (19.36), Garnet (4.77), Aragonite (4.17)	Olivine (0.12), Opx (52.88), Cpx (37.88), Garnet (8.32), Diamond (0.78), Magnetite (0.02)

Table S-5 *cont.*

Run	P GPa	T °C	logfO_2 ΔFMQ	pH	ΔlogfO_2	ΔpH	Initial Rock	Initial Mineralogy (vol %)	Final mineralogy (vol %)
47	5	1000	-5	5	0.71	0.17	Lherzolite + aragonite	Olivine (52.52), Opx (19.18), Cpx (19.36), Garnet (4.77), Aragonite (4.17)	Olivine (0.06), Opx (52.32), Cpx (38.69), Garnet (8.86), Diamond (0.07)
63	5	1000	-3	5	0.36	0.14	Dunite (no garnet)	Olivine (89.91), Opx (5.16), Cpx (4.93)	Olivine (0.17), Opx (66.38), Cpx (27.52), Garnet (3.20), Diamond (0.02), Magnetite (2.71)
69	5	1000	-3	5	0.42	0.15	Dunite + aragonite (no garnet)	Olivine (85.59), Opx (4.91), Cpx (4.70), Aragonite (4.81)	Olivine (0.18), Opx (25.59), Cpx (68.10), Garnet (3.11), Diamond (0.06), Magnetite (2.96)
75	**5**	**1000**	**-3**	**5**	**-0.06**	**0.14**	**Dunite + aragonite**	**Olivine (81.80), Opx (4.43), Cpx (4.62), Garnet (4.42), Aragonite (4.73)**	**Olivine (0.22), Opx (20.69), Cpx (62.87), Garnet (13.28), Diamond (0.06), Magnetite (2.88)**
76	5	1000	-4.1	5	-0.20	0.15	Dunite + aragonite	Olivine (81.80), Opx (4.43), Cpx (4.62), Garnet (4.42), Aragonite (4.73)	Olivine (0.19), Opx (47.13), Cpx (38.72), Garnet (12.59), Diamond (1.34), Magnetite (0.03)
77	5	1000	-5	5	0.71	0.16	Dunite + aragonite	Olivine (81.80), Opx (4.43), Cpx (4.62), Garnet (4.42), Aragonite (4.73)	Olivine (0.08), Opx (45.93), Cpx (40.11), Garnet (13.76), Diamond (0.12)
81	5	1000	-3	5	0.36	0.14	Harzburgite (no garnet)	Olivine (74.92), Opx (25.08)	Olivine (0.12), Opx (81.91), Cpx (13.07), Garnet (2.41), Diamond (0.03), Magnetite (2.46)
87	5	1000	-3	5	0.42	0.15	Harzburgite + aragonite (no garnet)	Olivine (71.41), Opx (23.91), Aragonite (4.68)	Olivine (0.17), Opx (53.15), Cpx (41.73), Garnet (2.27), Diamond (0.06), Magnetite (2.62)
93	**5**	**1000**	**-3**	**5**	**-0.06**	**0.14**	**Harzburgite + aragonite**	**Olivine (67.89), Opx (22.73), Garnet (4.78), Aragonite (4.60)**	**Olivine (0.15), Opx (46.34), Cpx (39.92), Garnet (10.92), Diamond (0.07), Magnetite (2.60)**

Table S-5 ***cont.***

Run	P GPa	T °C	logfO_2 ΔFMQ	pH	ΔlogfO_2	ΔpH	Initial Rock	Initial Mineralogy (vol %)	Final mineralogy (vol %)
94	5	1000	-4.1	5	-0.20	0.14	Harzburgite + aragonite	Olivine (67.89), Opx (22.73), Garnet (4.78), Aragonite (4.60)	Olivine (0.08), Opx (61.51), Cpx (26.29), Garnet (11.01), Diamond (1.11)
95	5	1000	-5	5	0.71	0.16	Harzburgite + aragonite	Olivine (67.89), Opx (22.73), Garnet (4.78), Aragonite (4.60)	Olivine (0.06), Opx (61.06), Cpx (26.88), Garnet (11.90), Diamond (0.10)
111	**5**	**1000**	**-3**	**5**	**-0.12**	**0.13**	**Dunite**	**Olivine (85.86), Opx (4.65), Cpx (4.85), Garnet (4.64)**	**Opx (58.29), Cpx (26.61), Garnet (12.40), Diamond (0.03), Magnetite (2.67)**
112	5	1000	-4.1	5	-0.30	0.16	Dunite	Olivine (85.86), Opx (4.65), Cpx (4.85), Garnet (4.64)	Olivine(0.07), Opx (72.10), Cpx (15.50), Garnet (12.33)
117	**5**	**1000**	**-3**	**5**	**-0.12**	**0.12**	**Harzburgite**	**Olivine (71.16), Opx (23.83), Garnet (5.01)**	**Olivine (0.13), Opx (73.46), Cpx (13.53), Garnet (10.40), Diamond (0.04), Magnetite (2.44)**
118	5	1000	-4.1	5	-0.30	0.15	Harzburgite	Olivine (71.16), Opx (23.83), Garnet (5.01)	Olivine (0.06), Opx (81.66), Cpx (7.42), Garnet (10.86)
125	5	1000	-3	5	0.49	0.17	Dunite + aragonite (10 vol.%)	Olivine (78.11), Opx (4.23), Cpx (4.41), Garnet (4.22), Aragonite (9.03)	Olivine (0.13), Cpx (82.68), Garnet (14.26), Magnetite (2.93)
126	5	1000	-3	5	0.64	0.20	Dunite + aragonite (15 vol.%)	Olivine (74.73), Opx (4.05), Cpx (4.22), Garnet (4.04), Aragonite (12.96)	Olivine (0.11), Cpx (82.08), Garnet (14.81), Magnetite (3.00)

Supplementary Information References

Bulanova, G.P., Walter, M.J., Smith, C.B., Kohn, S.C., Armstrong, L.S., Blundy, J., Gobbo, L. (2010) Mineral inclusions in sublithospheric diamonds from Collier 4 kimberlite pipe, Juina, Brazil: subducted protoliths, carbonated melts and primary kimberlite magmatism. *Contributions to Mineralogy and Petrology* 160, 489-510.

De Stefano, A., Kopylova, M.G., Cartigny, P., Afanasiev, V. (2009) Diamonds and eclogites of the Jericho kimberlite (Northern Canada). *Contributions to Mineralogy and Petrology*, 158, 295-315.

Dobosi, G., Kurat, G. (2010) On the origin of silicate-bearing diamondites. *Mineralogy and Petrology* 99, 29-42.

Gurney, J.J., Boyd, F.R. (1982) Mineral intergrowths with polycrystalline diamonds from the Orapa Mine, Botswana. *Carnegie Institute of Washington Yearbook* 81, 267-273.

Gurney, J.J., Harris, J.W., Rickard, R.S. (1984) Silicate and oxide inclusions in diamonds from the Orapa Mine, Botswana. In: Kornprobst, J. (Ed.) *Kimberlites II: The Mantle and Crust–Mantle Relationships*. Elsevier, Amsterdam, 3-9.

Huang, F., Sverjensky, D.A. (2019) Extended Deep Earth Water Model for predicting major element mantle metasomatism. *Geochimica et Cosmochimica Acta*, 254, 192-230.

Jacob, D.E., Viljoen, K.S., Grassineau, N., Jagoutz, E. (2000) Remobilization in the cratonic lithosphere recorded by polycrystalline diamond (framesite). *Science* 289, 1182-1185.

Kessel, R., Pettke, T., Fumagalli, P. (2015) Melting of metasomatized peridotite at 4–6 GPa and up to 1200 °C: an experimental approach. *Contributions to Mineralogy and Petrology* 169, 37.

Mikhail, S., McCubbin, F.M., Jenner, F.E., Shirey, S.B., Rumble, D., Bowden, R. (2019) Diamondites: evidence for a distinct tectono-thermal diamond-forming event beneath the Kaapvaal craton. *Contributions to Mineralogy and Petrology* 174, 71.

Miller, C.E., Kopylova, M., Smith, E. (2014) Mineral inclusions in fibrous diamonds: constraints on cratonic mantle refertilization and diamond formation. *Mineralogy and Petrology* 108, 317-331.

Shock, E.L. Helgeson, H.C. (1988) Calculation of the thermodynamic and transport properties of aqueous species at high pressures and temperatures: Correlation algorithms for ionic aqueous species and equation of state predictions to 5 kb and 1000 °C. *Geochimica et Cosmochimica Acta* 52, 2009-2036.

Shock, E.L., Sassani, D.C., Willis, M., Sverjensky, D.A. (1997) Inorganic Species in Geologic Fluids: Correlations among Standard Molal Thermodynamic Properties of Aqueous Cations, Oxyanions, Acid Oxyanions, Oxyacids and Hydroxide Complexes. *Geochimica et Cosmochimica Acta* 61, 907-950.

Sobolev, N.V., Logvinova, A.M., Zedgenizov, D.A., Pokhilenko, N.P., Malygina, E.V., Kuzmin, D.V., Sobolev, A.V. (2009) Petrogenetic significance of minor elements in olivines from diamonds and peridotite xenoliths from kimberlites of Yakutia. *Lithos* 112, 701-713.

Stachel, T., Harris, J.W. (2008) The origin of cratonic diamonds – constraints from mineral inclusions. *Ore Geology Review* 34, 5-32.

Sverjensky, D.A. (2019) Thermodynamic modelling of fluids from surficial to mantle conditions. *Journal of the Geological Society* 176, 348-374.

Sverjensky, D.A., Shock, E.L., Helgeson, H.C. (1997) Prediction of the thermodynamic properties of aqueous metal complexes to 1,000 °C and 5.0 kb. *Geochimica et Cosmochimica Acta* 61, 1359-1412.

Tappert, R., Stachel, T., Harris, J.W., Shimizu, N., Brey, G.P. (2005) Mineral inclusions in diamonds from the Panda kimberlite, Slave Province, Canada. *European Journal of Mineralogy* 17, 423-440.

Tappert, R., Foden, J., Stachel, T., Muehlenbachs, K., Tappert, M., Wills, K. (2009) The diamonds of South Australia. *Lithos* 112, 806-821.

Wolery, T.J. (1983) *EQ3NR, A computer program for geochemical aqueous speciation-solubility calculations: User's guide and documentation*. UCRL-53414. Lawrence Livermore National Laboratory, University of California, Livermore, California.

Wolery, T.J. (1984) *EQ6, A computer program for reaction-path modelling of aqueous geochemical systems: User's guide and documentation*. UCRL-51. Lawrence Livermore National Laboratory, University of California, Livermore, California.

Wolery, T.J. (1992) *EQ3/6: A software package for geochemical modeling of aqueous systems: package overview and installation guide (version 7.0)*. Lawrence Livermore National Laboratory, University of California, Livermore, California.

Viljoen, K., Phillips, D., Harris, J.W, Robinson, D. (1999) Mineral inclusions in diamonds from the Venetia kimberlites, Northern Province, South Africa. *International Kimberlite Conference: Extended Abstracts* 7, 943-945.